9870–9880 *Nucleic Acids Research, 2013, Vol. 41, No. 21* *Published online 22 August 2013*
doi:10.1093/nar/gkt735

One antitoxin—two functions: SR4 controls toxin mRNA decay and translation

Natalie Jahn and Sabine Brantl*

AG Bakteriengenetik, Lehrstuhl für Genetik, Friedrich-Schiller-Universität Jena, Philosophenweg 12, Jena D-07743, Germany

Received July 1, 2013; Revised July 24, 2013; Accepted July 25, 2013

ABSTRACT

Type I toxin–antitoxin systems encoded on bacterial chromosomes became the focus of research during the past years. However, little is known in terms of structural requirements, kinetics of interaction with their targets and regulatory mechanisms of the antitoxin RNAs. Here, we present a combined *in vitro* and *in vivo* analysis of the *bsrG*/SR4 type I toxin–antitoxin system from *Bacillus subtilis*. The secondary structures of SR4 and *bsrG* mRNA and of the SR4/*bsrG* RNA complex were determined, apparent binding rate constants calculated and functional segments required for complex formation narrowed down. The initial contact between SR4 and its target was shown to involve the SR4 terminator loop and loop 3 of *bsrG* mRNA. Additionally, a contribution of the stem of SR4 stem-loop 3 to target binding was found. On SR4/*bsrG* complex formation, a 4 bp double-stranded region sequestering the *bsrG* Shine Dalgarno (SD) sequence was extended to 8 bp. Experimental evidence was obtained that this extended region caused translation inhibition of *bsrG* mRNA. Therefore, we conclude that SR4 does not only promote degradation of the toxin mRNA but also additionally inhibit its translation. This is the first case of a dual-acting antitoxin RNA.

INTRODUCTION

Toxin–antitoxin (TA) loci encode two-component systems that consist of a stable 'toxin' whose ectopic overexpression either kills cells or confers growth stasis, and an unstable 'antitoxin' [reviewed in (1)]. In type I TA systems, the antitoxin is a small RNA, and the toxin mRNA encodes a hydrophobic peptide. Initially, these systems have been discovered on plasmids [e.g. *hok*/Sok on *Escherichia coli* plasmid R1 (2), *fst*/RNAII on *Enterococcus faecalis* plasmid pAD1 (3)], where they act as post-segregational killing (PSK) systems to prevent plasmid loss at cell division. Later, chromosomally encoded type I TA systems were found and investigated, among them are *tisB*/IstR1 (4,5), *symE*/SymR (6), *ibs*/Sib and *shoB*/OhsC [(7,8), reviewed in (9)] from *E. coli* and *txpA*/RatA (10,11) and *bsrG*/SR4 (12) from *Bacillus subtilis*. Numerous other systems were predicted and await experimental confirmation (13).

The biological role of chromosome-encoded TA systems is far less clear. Recently, for *E. coli tisB*/IstR1, a role in persister formation has been found (14). In *B. subtilis*, 14 type I TA systems were postulated (15). In five of them, the experimentally confirmed (*txpA, bsrG, yonT*) or putative (*bsrE, bsrH*) toxin genes are located on prophages and suggested to be required for prophage maintenance similar to the function of plasmid-encoded PSK (15).

In all cases examined so far, the interaction between RNA antitoxin and toxin mRNA either leads to inhibition of translation or promotes the degradation of the toxin mRNA [reviewed in (16,17)].

However, *cis*-encoded antisense RNAs, to which type I antitoxins belong, can use a much broader variety of regulatory mechanisms. These include translation inhibition by direct pairing to the target RNA SD sequence [*E. coli symE*/SymR (6)], translation attenuation [plasmid pSK41 (18)], transcriptional attenuation [plasmids pIP501 and pT181 (19–21), inhibition of pseudoknot formation [IncIα/IncB plasmids (22)], transcriptional interference [*Clostridium acetobutylicum ubiG* operon (23)], mRNA stabilization owing to a processing event [*E. coli* GadY/*gadWX* (24)] and mRNA degradation [*txpA*/RatA, reviewed in (16,17)]. To our knowledge, no *cis*-encoded antisense RNA examined so far has two clearly separable functions.

Recently, we published with *bsrG*/SR4 the first temperature-dependent type I TA system (12). The ≈294 nt *bsrG* RNA encodes a 38 aa toxic hydrophobic peptide that causes cell lysis on agar plates. Half-life measurements in wild-type and knockout strains demonstrated that the ≈180 nt antitoxin SR4 that is complementary to the 3′ end of *bsrG* mRNA promotes toxin mRNA degradation by an RNase III-dependent mechanism. Exoribonuclease

*To whom correspondence should be addressed. Tel: +49 3641 949570; Fax: +49 3641 949302; Email: Sabine.Brantl@rz.uni-jena.de

R and endoribonuclease Y are responsible for *bsrG* RNA and SR4 degradation, whereas PnpA processes three SR4 precursors to the mature RNA. Transcriptional *lacZ* fusions indicated that the antitoxin promoter is significantly stronger than the toxin promoter. BsrG expression increases at the onset of stationary phase, and the amount of *bsrG* RNA decreases drastically at heat shock (48°C) due to the 3-fold increased degradation of toxin RNA at high temperatures (12).

Only for *hok*/Sok and *fst*/RNAII, two plasmid-encoded TA systems, detailed *in vitro* and *in vivo* analyses on secondary structures of antitoxin and toxin mRNA and their complex as well as on the binding pathway and mechanism of action of the antitoxin RNAs have been performed [summarized in (25–27)]. In both cases, the antitoxin RNA inhibits translation initiation of the toxin mRNA. However, although Sok interacts with the 5′ region of *hok* mRNA (28,29), RNAII uses two base-paired regions located apart, one at the 3′ end, the other at the 5′ end, to target the *fst* toxin mRNA (30,31). The *ibs*/Sib TA systems from *E. coli* (7) were the first chromosomally encoded type I TA systems, for which the interaction between antitoxin and toxin RNAs was investigated *in vitro* (8). Two target recognition domains (TRD) of the Sib antitoxins were identified, which are responsible for the recognition of the cognate toxin mRNAs (8). Recently, the secondary structures of RatA and *txpA* RNA and their complex were determined, but binding rate constants or binding pathway have not been elucidated so far (11).

Here, we provide a combined *in vitro* and *in vivo* characterization of SR4, *bsrG* RNA and the SR4/*bsrG* complex. We determined the secondary structures of both RNAs as well as that of the complex. Furthermore, we elucidated the region of initial contact between RNA antitoxin and toxin mRNA and the mechanism of SR4/*bsrG* pairing using complex formation studies with full-length and truncated SR4 and *bsrG* RNA pairs, *in vivo* studies with plasmids expressing SR4 and *bsrG* derivatives as well as time-course experiments. By expressing *bsrG* RNA derivatives that contain SD sequences within short or extended double-stranded regions, we demonstrate that the SR4/*bsrG* RNA pairing does not only negatively affect *bsrG* RNA stability but also inhibits translation initiation.

MATERIALS AND METHODS

Enzymes and chemicals

Chemicals used were of the highest purity available. Taq DNA polymerase was purchased from Roche and Firepol polymerase from Solis Biodyne. T7 RNA polymerase, RNases T1 and V1 from AMBION, RNase T2 from Sigma and nuclease S1 from Fermentas were used. RNA ligase and the *in vitro*-translation kit PURExpress were from New England Biolabs and ThermoScript reverse transcriptase from Invitrogen.

Strains, media and growth conditions

Bacillus subtilis strains DB104 (32) and DB104(*Δsr4ΔbsrG*::*cat*) (12) and *E. coli* strain TG1 were grown in complex TY medium (33).

In vitro transcription and secondary structure analysis of SR4, *bsrG* RNA and the SR4/*bsrG* RNA complex

In vitro transcription and partial digestions of *in vitro* synthesized 5′-end labelled SR4 and *bsrG* RNA species with ribonucleases T1 (1 U/μl), T2 (22 U/μl) and V (0.1 U/μl) and nuclease S1 (100 U/μl) were carried out as described (34). Additionally, *bsrG* RNA was 3′-end labelled with [^{32}P]pCp and RNA ligase for 30 min at 37°C. For the analysis of SR4/*bsrG* complexes with T1 and T2 either SR4 or *bsrG* RNA were 5′-end labelled, and a 2.5–60-fold excess of the cold complementary RNA was added before RNase digestion. Secondary structure probing with chemical probes (CMCT and DMS) using 2 pmol of unlabelled *bsrG* RNA in a total volume of 20 μl was carried out as described previously (20) with following modifications: The RT reactions were performed with different 5′ labelled primers (see Supplementary Table S1) and with ThermoScript reverse transcriptase (15 U/μl) for 40 min at 60°C followed by 20 min at 65°C.

Time-course experiment

In vitro-synthesized 5′ labelled SR4 (0.33 μM) was incubated with a 30-fold excess of unlabelled *bsrG* RNA, time samples were taken and 50-fold diluted to prevent further complex formation during the subsequent partial digestion with RNases T1 (10^{-2} U) and T2 (2.2×10^{-2} U). The reaction was stopped by ethanol precipitation, and RNAs dissolved in 5 μl of H_2O and 5 μl of formamide loading dye. Samples were separated on an 8% denaturing PAA gel and subsequently analysed by PhosphorImaging.

Analysis of RNA-RNA complex formation

Both *bsrG* RNA and SR4 were either synthesized *in vitro* from PCR-generated template fragments with primer pairs or generated by hybridization of oligonucleotides (see Supplementary Table S1). SR4/*bsrG* complex formation studies were performed as described previously (33).

Preparation of total RNA and northern blotting

Preparation of total RNA and northern blotting were carried out as described previously (35).

Construction of plasmids for the *in vivo* assays

Plasmids pUCBSR4_4 to pUCBSR4_9 used for constitutive overexpression of different SR4 species from a high-copy number plasmid ($\approx$50 copies/cell) in *B. subtilis* under their own promoters were generated by cloning BamHI/HindIII fragments obtained by PCR with different primer pairs (see Supplementary Table S1) on chromosomal DNA from *B. subtilis* strain DB104 into the BamHI/HindIII digested vector pUCB2. The insert of pUCBSR4_4 lacking nt 1–89 of *sr4* was generated by a two-step PCR with primer pairs SB1605/SB1973 and SB1606/SB1974 in the first two reactions and primer pair SB1605/SB1606 in the second PCR reaction. The PCR fragment of pUCBSR4_6 lacking nt 1–110 of *sr4* was also generated with a two-step PCR using primer pairs SB1605/SB1975 and SB1995/SB1976 for the first reactions followed by a second PCR with the primer pair

SB1605/SB1995. The downstream primer includes the heterologous *bsrF* transcription terminator. Plasmid pUCBSR4_8 was constructed by inserting a BamHI/HindIII fragment containing an altered sequence of loop 4 of *sr4* obtained by PCR on chromosomal DNA with primer pair SB1605/SB2041 into the BamHI/HindIII digested pUCB2 vector. The same approach was used to construct pUCBSR4_9 (SB1605/SB2054) lacking nt 132–180. The downstream primer SB2054 allowed to include the *bsrF* terminator at the truncated 3′-end.

Plasmids pGKBG4 and pGKBG5 used for constitutive overexpression of truncated *bsrG* species lacking nt 179–294 from an intermediate copy number plasmid (≈15 copies/cell) in *B. subtilis* under their own promoters were generated by cloning BamHI/HindIII fragments obtained by PCR on plasmid pGKBG (12) with different primer pairs into the BamHI/HindIII digested vector pGK14. The insert of pGKBG4 was generated by a PCR reaction with primer pair SB1405/SB2113. The fragment of plasmid pGKBG5 containing alterations at nt 34–36 of *bsrG* was obtained by a two-step PCR with primer pairs SB2113/SB2114 and SB1405/SB2115 followed by a second PCR reaction with outer primers SB1405/SB2113. The downstream primer SB2113 allowed to include the *bsrF* terminator at the truncated 3′ end of *bsrG*. All PCR generated inserts were confirmed by sequencing. All plasmids are listed in Supplementary Table S2.

RESULTS

Secondary structures of SR4 and *bsrG* mRNA

As computer-predicted RNA structures often deviate from experimentally determined ones [e.g. RNA III of plasmid pIP501 (19,20), RNAI/RNAII of plasmid pT181 (21) or SR1 from *B. subtilis*, (36)], we performed limited digestions with structure-specific ribonucleases to determine the secondary structure of SR4. Full-length SR4 (183 nt) as well as 5′ truncated $SR4_{90\text{-}183}$ were 5′-end labelled, gel-purified and treated with RNases T1 (cleaves 3′ of unpaired G residues), T2 (unpaired nucleotides with a slight preference for A residues), V1 (double stranded and stacked regions) and nuclease S1 (single-stranded nucleotides). Figure 1A shows the analysis of SR4, and Figure 1B displays the schematic presentation of the SR4 structure derived from the cleavage data. The experimentally determined structure comprises four stem-loops SL1, SL2, SL3 and SL4 interrupted by short unpaired regions, SL4 being the terminator stem-loop. Apart from the lack of a small stem-loop within the first 20 nt and the size and structure of loop 1, the experimentally determined structure coincided well with the structure predicted previously by the DINAMelt Webserver (12). Structure probing of full-length SR4 and truncated $SR4_{90–183}$ revealed a modular structure, i.e. the four stem-loops fold independently. This information was used to assess complex formation (see later in the text).

The secondary structure of the full-length *bsrG* (296 nt) mRNA was determined by a combination of enzymatic and chemical structure probing as described in 'Materials and Methods' section. For enzymatic probing, 5′ and 3′ labelled RNA species were used. The corresponding gels are shown in Supplementary Figure S1, the schematic representation of the *bsrG* structure in Figure 2. *bsrG* RNA is highly structured and does barely contain single-stranded regions: The 5′ nt 1–35 and the 3′ nt 232–262 base pair in the long helix P1, which is divided by bulged-out nt into five sub-helices. P1 branches on top in stem-loop structures SL1 to SL3, the latter two comprising large internal loops. The *bsrG* SD sequence is located in a 4 bp double-stranded region in the stem of SL1. Start and stop codons are situated at the 5′ base of SL2 and the 5′ part of SL3, respectively. The terminator stem-loop SL4 comprises nt 263–296 and is separated from P1 by only one unpaired nucleotide.

Secondary structure of the SR4/*bsrG* complex

To investigate conformational changes in the secondary structures of SR4 and *bsrG* RNA on pairing, the secondary structure of the SR4/*bsrG* RNA complex was determined. To ascertain alterations in the *bsrG* RNA structure, 5′ labelled *bsrG* RNA was incubated with an excess of unlabelled SR4, the complex was allowed to form for 5 min at 37°C and, subsequently, partially digested with RNases T1 and T2 (Figure 3A top). In parallel, 5′ labelled SR4 was incubated with an excess of unlabelled *bsrG* RNA and treated likewise (Figure 3A, bottom). Figure 3B shows the schematic representation of the complex. As expected, no alteration in SL1 of SR4 was observed, as this part of the antitoxin RNA is not complementary to *bsrG* RNA. By contrast, the complementary region of SR4 and *bsrG* RNA was found to be completely double stranded as indicated by significantly reduced cleavages with RNases T1 and T2 (Figure 3B, top). Interestingly, the 5′ 60 nt of *bsrG* RNA that are not complementary to SR4 underwent significant structural alterations, whereas SL3 of unbound *bsrG* RNA remained unchanged. Nucleotides 1–33 that were base paired in helix P1 of free *bsrG* RNA were found to be single stranded in the complex, and nt 34–57 formed a novel small stem-loop (SL1) comprising the SD sequence. Surprisingly, the double-stranded region with the SD sequence that encompasses 4 GC bp in free *bsrG* RNA was extended to 8 bp in the complex with SR4 (Figure 3B, bottom).

Binding assays of wild-type and truncated SR4/*bsrG* mRNA pairs indicate that SL4 and part of SL3 of SR4 are required for efficient pairing

To analyse the kinetics of stable complex formation *in vitro*, we first studied binding between labelled full-length SR4 and unlabelled full-length *bsrG* RNA and *vice versa* by gel-shift assay as described in 'Materials and Methods' section. An overview of calculated second-order binding rate constants (k_{app}) is presented in Figure 4A, and representative gel-shift experiments are shown in Figure 4B. For the full-length SR4/*bsrG* pair, we determined a k_{app} value of $\approx 6 \times 10^5\,M^{-1}s^{-1}$ independent of which of the interacting RNAs was labelled and which was provided unlabelled in excess (see also Supplementary Figure S2). This k_{app} value is in the

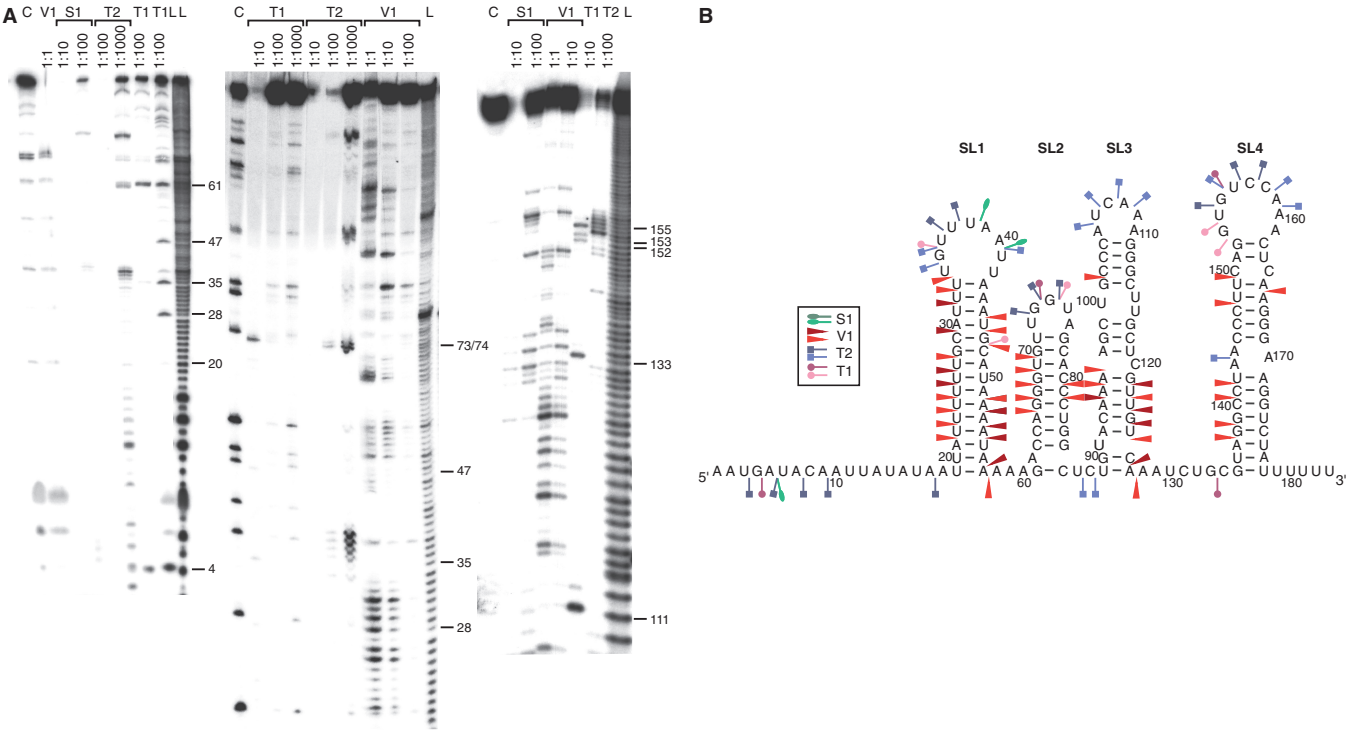

Figure 1. Secondary structure of SR4 (183 nt). (**A**) Secondary structure probing of SR4 with RNases. Purified, 5′ labelled wild-type $SR4_{1–183}$ and $SR4_{90–183}$ (right panel) were subjected to limited cleavage with the RNases indicated. The digested RNAs were separated on 15% (left) or 8% denaturing gels. Autoradiograms are shown. C, control without RNase treatment; L, alkaline ladder; T1L, T1 digestion under denaturing conditions. Nucleotide positions are indicated. (**B**) Proposed secondary structure of SR4. A structure consistent with the cleavage data in Figure 1A is depicted. Major (dark symbols) and minor (light symbols in the same colour) cuts are indicated (see box). The four stem-loops SL1, SL2, SL3 and SL4 are indicated.

same order of magnitude as those determined for other sense/antisense pairs with long stretches of complementarity [reviewed in (37)]. Next, we introduced different truncations within the antisense RNA SR4 to assay, which structural elements are required for stable complex formation. As expected from previous *in vivo* experiments (12), $SR4_{1\text{-}90}$ comprising only SL1 and SL2 was not able to form a complex with full-length *bsrG* RNA, although it contains the first of the three stem-loops complementary to *bsrG* RNA. $SR4_{1\text{-}131}$ containing SL1, SL2 and SL3, but lacking the terminator stem-loop SL4, was 10-fold impaired in stable pairing. By contrast, $SR4_{90\text{-}183}$ comprising SL3 and SL4 formed a complex with *bsrG* RNA as efficient as full-length SR4, indicating that the latter region is sufficient for stable pairing, whereas neither SL3 ($SR4_{77–135}$) nor SL4 ($SR4_{128–180}$) alone was sufficient. Interestingly, the 3′ half of SL3 seemed to be adequate in addition to entire SL4, as $SR4_{111–183}$ bound with a wild-type k_{app} of $6 \times 10^5\,M^{-1}s^{-1}$. Further shortening of this 3′ half, however (see $SR4_{115–180}$), yielded a poor binder. This suggested a contribution of nt 111–115 (GGGC) to efficient complex formation. To further investigate the role of this sequence to stable binding, the stem region of SL3 was inverted horizontally to remain double stranded (see Figure 4), topped by a wild-type L3. This mutant ($SR4_{90–180}$-invert1) bound 5-fold worse than full-length SR4. When the upper part of stem 3 containing nt 111–115 was kept in wild-type orientation and only the lower part inverted ($SR4_{90–180}$-invert2), pairing was not improved, but ≈6-fold lower k_{app} values calculated (Figure 4A). This indicates that the particular sequence GGGC was not required. Furthermore, an exclusive exchange of the SR4 L3 sequence did not affect binding (Figure 4A). These results demonstrate that intermolecular helix formation progresses from L4 in 5′ direction via complementary regions towards L3. The deletion of the *bsrG* terminator stem-loop did not alter significantly k_{app}, confirming that the contact between SL2 of SR4 and the *bsrG* terminator is not important (Supplementary Figure S2).

In summary, we can conclude that SL4 of SR4 and a longer complementary region 5′ of it are required for stable pairing between SR4 and *bsrG* RNA.

The initial contact between SR4 and *bsrG* mRNA occurs between terminator loop L4 of SR4 and loop 3 of *bsrG* mRNA

To narrow down the region of the initial contact between the antitoxin SR4 and the *bsrG* toxin mRNA, we analysed stable pairing between RNAs carrying several nucleotide exchanges in SL4 of SR4 and/or in loop L3 of *bsrG*. First, the entire sequence of loop L4 of SR4 (nt 153–161) was altered resulting in a 10-fold impaired binding to *bsrG* RNA. This substantiates the importance of L4 of

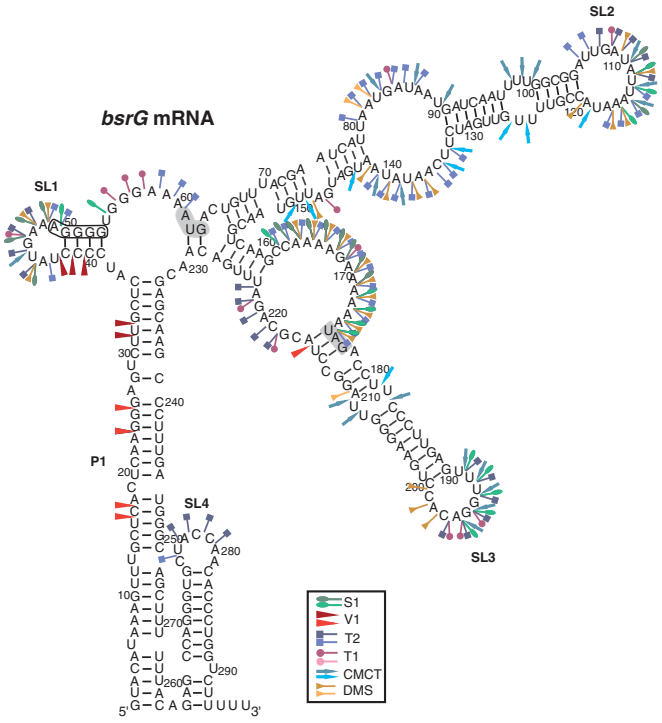

Figure 2. Secondary structure of *bsrG* mRNA (296 nt). A structure consistent with the cleavage data in Supplementary Figure S1 and additional experiments (data not shown) is depicted. Major and minor cuts or modifications are indicated by coloured dark and light symbols (see box). The long double-stranded helix P1 and the four main stem-loops SL1 to SL4 are indicated. The SD sequence of the *bsrG* ORF is boxed, and start and stop codon are shaded in grey.

SR4 for the recognition of *bsrG* RNA. When a shortened SR4 mutant ($SR4_{111–180}$) with nucleotide exchanges in L4, but comprising only the minimal length required for efficient pairing, was analysed, k_{app} decreased even 100-fold. Likewise, the exchange of L3 of *bsrG* RNA that is complementary to L4 of SR4 impaired complex formation 10-fold, underlining the importance of the contact between this loop and the terminator loop L4 of SR4 (Supplementary Figure S2). A compensatory mutation restoring complementarity between L3 of *bsrG* and L4 of SR4 yielded the initial pairing rate constant (Supplementary Figure S2).

Additionally, a time-course experiment as described in 'Materials and Methods' section was performed to assay the sequential pairing between the complementary regions of antisense and sense (toxin) RNA. As shown in Figure 5, T1 and T2 cleavage signals specific for L4 disappeared already after 1 and 30 s, whereas those for L3 were weak, but still visible after 90 and 360 s. Only a marginal reduction was detectable for L2 complementary to the *bsrG* terminator stem-loop, which confirmed the data of the binding assays that showed no contribution of SL2 to efficient pairing. Moreover, the single-stranded region between SL3 and SL4 of SR4 was converted into a double strand before L3 (see T1 cut at G_{133} in Figure 5), which indicates that the intermolecular helix progresses from L4 via this single strand towards L3. As expected, no alterations in the cleavage pattern were observed for L1 that is not complementary to *bsrG* RNA. From the results of the binding assays and the time-course experiment, we infer that the initial contact between SR4 and *bsrG* RNA occurs between L4 of SR4 and loop L3 of *bsrG* RNA, followed by helix progression via the single strand between L4 and L3 to an interaction at loop 3 of SR4 and, much later, at L2 of SR4 and L4 of *bsrG* RNA.

In vivo studies corroborate the *in vitro* data

To corroborate our *in vitro* data *in vivo*, *sr4* was expressed from multi-copy plasmid pUCB2 (≈50 copies/cell) and *bsrG* from plasmid pGK14 (≈15 copies/cell) in a chromosomal *Δsr4*/*ΔbsrG* background as described recently (12). Insert-free plasmid pUCB2 served as control. Supplementary Figure S3 shows that all SR4 species are expressed at approximately the same levels. Lysis on agar plates was assayed after overnight incubation at 37°C followed by incubation at room temperature. As summarized in Figure 6, full-length SR4 (pUCBSR4_1), SR4 lacking SL1 (pUCBSR4_3) or both SL1 and SL2 (pUCBSR4_4) and SR4 comprising only SL4 and the 3′ part of SL3 (pUCBSR4_6) were equally able to inhibit BsrG-induced lysis. By contrast, SR4 containing only SL1 and SL2 followed by the *bsrF* terminator (pUCBSR4_2) behaved as the insert-free pUCB2 vector, i.e. full lysis occurred after 17 h incubation. These results coincide well with the data from the binding assays. Plasmid pUCBSR4_8 expressing full-length SR4 with exchanged loop 4 sequence could be established in *Δsr4*/*ΔbsrG*, but was impaired in lysis compensation (++). Likewise, SR4 lacking SL4 (pUCBSR4_9) was only able to delay lysis for 24 h, but not to prevent it (+). These results confirmed our *in vitro* data and demonstrated the importance of SL4 and a contribution of the 3′ half of SL3 to pairing with *bsrG* RNA and, consequently, the prevention of the toxic effect of BsrG *in vivo*.

SR4 affects both degradation and translation of *bsrG* mRNA

The results of the secondary structure probing of the SR4/*bsrG* RNA complex revealed an extension of the double-stranded region sequestering the SD sequence in free *bsrG* RNA from 4 to 8 bp (Figure 3). This prompted us to investigate whether this alteration does affect *bsrG* translation. As a translational *lacZ* fusion did not allow measuring any β-galactosidase activity in the presence or absence of SR4 (12), we used an *in vitro* translation assay to analyse translation of wild-type and mutated *bsrG* RNA in the presence of ^{35}S-[Met]. With wild-type *bsrG* RNA, no translation product could be observed, even after optimizing all reaction conditions and a 2 d exposure in the PhosphorImager (Supplementary Figure S4B). This was in agreement with the previous β-galactosidase measurements. Shortening of the double-stranded region sequestering the SD sequence from 4 to 2 bp or substitution of the 4 GC by GU bp yielded weak translation products. Only mutations that prevented the formation of any double-stranded region (Supplementary Figure S4B, lane 4: SD sequence AGGGG now fully single stranded) resulted in a significant amount of translation product. Therefore, an *in vitro* translation assay could not be used to investigate an

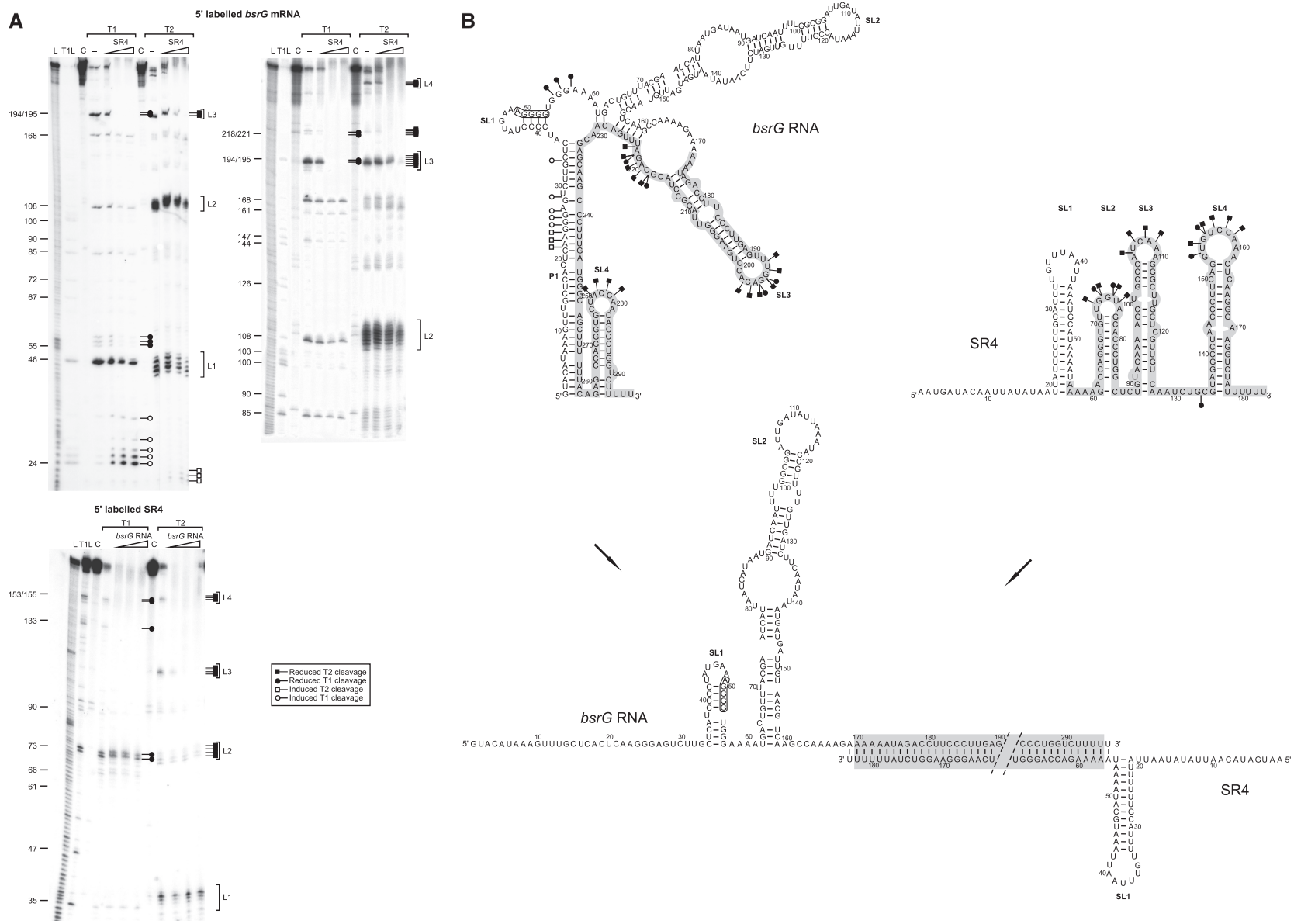

Figure 3. Secondary structure of the SR4/*bsrG* complex. (**A**). Secondary structure probing of the SR4/*bsrG* complex. 80 nM of purified, 5′ labelled *bsrG* RNA (above) or 5′ labelled SR4 (below) were incubated with increasing amounts of the complementary unlabelled RNA (200 nM, 1.6 μM, 4.8 μM), the complex allowed to form for 5 min at 37°C and subjected to limited cleavage with T1 (10^{-2} U/μl) and T2 (2.2×10^{-2} U/μl). The digested RNAs were separated on 8% denaturing gels. Autoradiograms are shown. C, control without RNase treatment; L, alkaline ladder; T1L, T1 digestion under denaturing conditions. Nucleotide positions are included. Altered T1, T2 cleavages are indicated by the symbols shown in the box. (**B**). Alterations in the structures of *bsrG* RNA and SR4 on complex formation. Altered cleavages are shown in the *bsrG* RNA and the SR4 structures separately. The *bsrG* SD sequence is boxed. Complementary regions are shaded in grey. The proposed secondary structure of the *bsrG* RNA/SR4 complex is shown below. The complementary region was found to be completely double stranded; therefore, only part of it is shown and instead of the rest, two dashed lines were included.

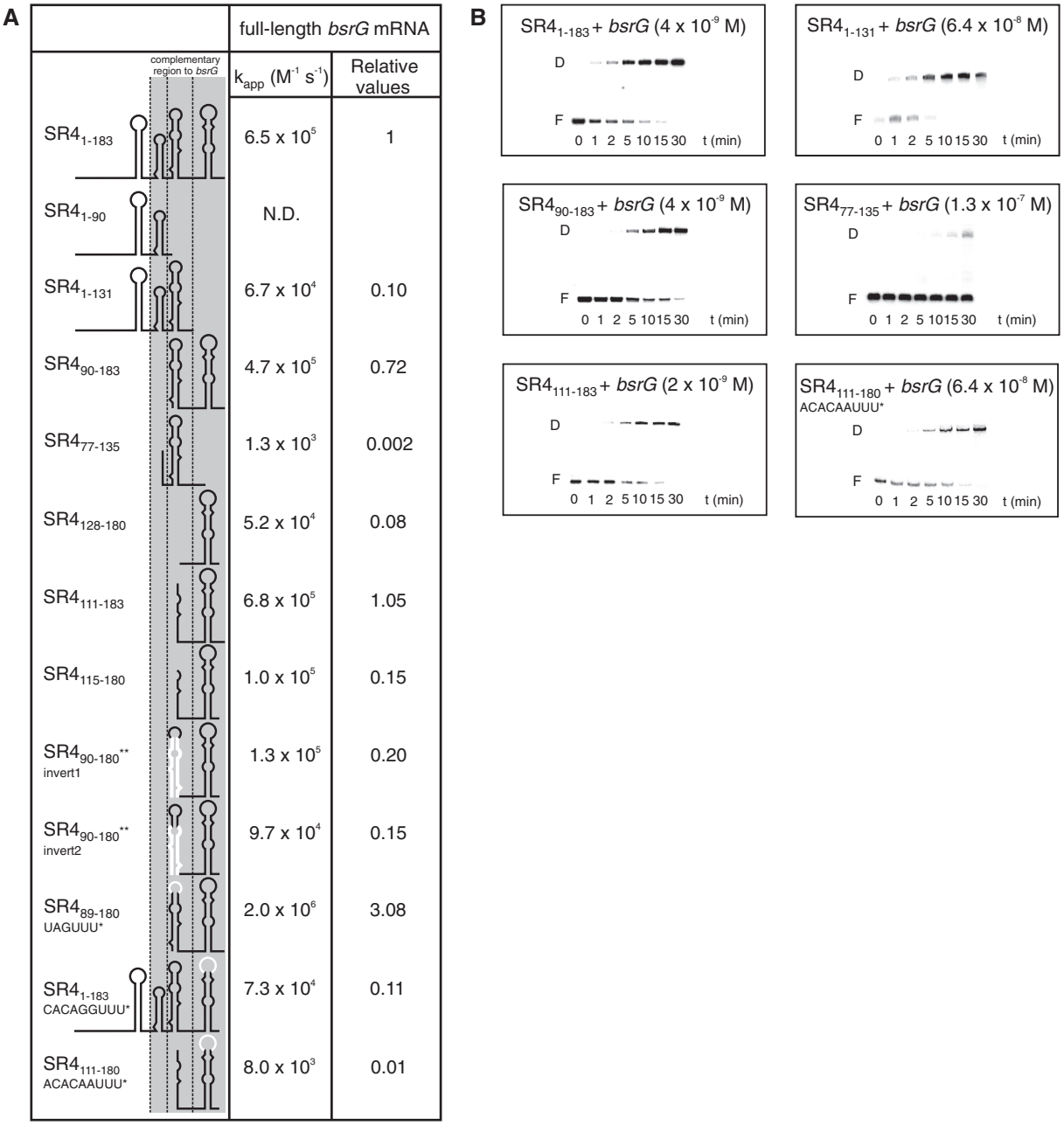

Figure 4. Binding assays of wild-type and truncated SR4/*bsrG* RNA pairs. Binding experiments were performed as described in 'Materials and Methods' section. (**A**) Summary of pairing rate constants (k_{app}). The conformation of the used SR4 species is shown schematically in the left column, and sequence alterations are indicated. The k_{app} values were calculated as described previously (19). (**B**) Representative binding assays with wild-type and truncated/mutated SR4 derivatives. Wild-type and truncated/mutated SR4 species were 5′ labelled with γ-[^{32}P]-ATP and used in at least 10-fold lower equimolar amounts compared with the full-length *bsrG* RNA. The concentration of unlabelled wild-type *bsrG* RNA species is indicated. F, free labelled RNA, D duplex between SR4 and *bsrG* RNA. Asterisk denotes the sequence by which the wild-type sequence of SR4 was replaced (white thin line). Double asterisk indicates that the entire (nt 89–104 changed into 11–127 and vice versa) or part (nt 89–100 changed into 115–127 and vice versa) of the stem-region of SL3 was inverted (thick white lines).

influence of SR4 on translation of wild-type *bsrG* RNA. As toeprinting assays did also not yield any toeprint with wild-type *bsrG* RNA (not shown), we resorted to an indirect approach: We constructed two mutant plasmids, one that mimics the SL1 structure comprising the SD sequence of *bsrG* in the absence of SR4 (plasmid pGKBG5), the other one mimics the SL1 structure induced by binding of SR4 (plasmid pGKBG4). Both plasmids allow for constitutive overexpression of these truncated *bsrG* species containing the toxin ORF at intermediate copy number in *B. subtilis*. As they lack the 3′ nt complementary to SR4, the mutated *bsrG* RNAs expressed from these plasmids are not sensitive to SR4. For accurate transcription termination, the *bsrF* terminator was added at the 3′ end (Figure 7A). The structure of the mutated RNAs was confirmed experimentally (Supplementary Figure S4). Plasmid pGKBG5 does only

allow expression of a *bsrG* RNA with an SD sequence in a 4 bp double-stranded region as in the absence of SR4 (see Figure 2B). By contrast, plasmid pGKBG4 allows expression of a *bsrG* RNA whose SD sequence is located in an 8 bp double-stranded region. After transformation with either plasmid, only pGKBG4 could be established in the *Δsr4*/*ΔbsrG* strain, where it yielded lysis after overnight incubation at 37°C, whereas plasmid pGKBG5 could not be established in this strain. Lysis can be observed because the degradation of *bsrG* RNA by RNase III that is induced by SR4 in the wild-type case (12) cannot occur.

Apparently, the formation of an extended 8 bp region sequestering the *bsrG* SD inhibits toxin translation to a certain degree, whereas the 4 bp region is unable to do so. As the binding of SR4 to *bsrG* RNA induces the extension of the 4 bp to an 8 bp double-stranded region, we conclude that SR4 does not only promote degradation of *bsrG* RNA as shown before (12) but also additionally inhibits *bsrG* translation by introducing a structural change that impedes the access of ribosomes.

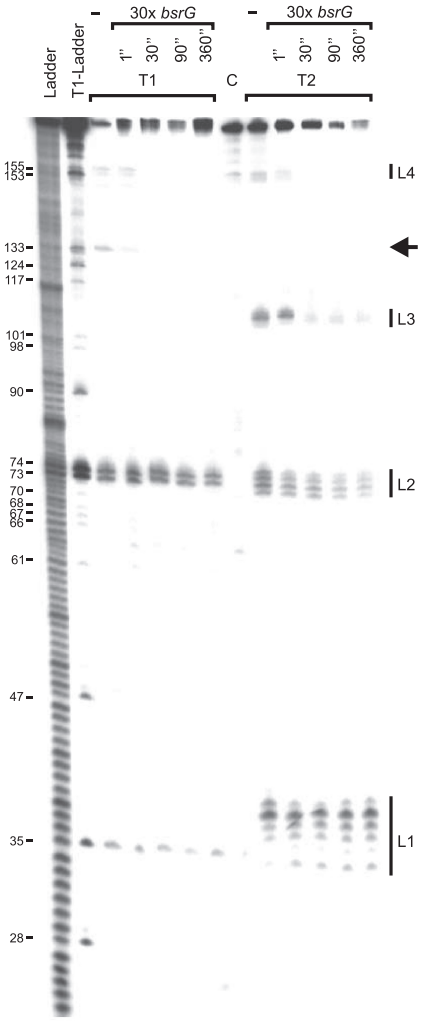

Figure 5. Time-course of interaction between SR4 and *bsrG* RNA. Autoradiogram of the time course experiment performed as described in 'Materials and Methods' section. C, control; L, alkaline ladder; T1L, T1 ladder. The loop regions L1 to L4 of SR4 are indicated at the right. Arrow: G133.

DISCUSSION

Although with *hok*/Sok and *fst*/RNAII two plasmid-encoded type I TA systems have been characterized in great detail in terms of the antitoxin/toxin RNA binding pathway and the inhibitory mechanism used by the antitoxin [summarized in (16,26,27,38)], relatively little is known about such systems present on bacterial chromosomes. Sok binds at the *mok*/*hok* SD sequence and inhibits ribosome binding (28), and RNAII interacts with 5′ and 3′ regions of *fst* RNA keeping it in a translationally inactive complex (39). By contrast, SR4 and *bsrG* RNA pair at their 3′ ends, and SR4 binding promotes *bsrG* mRNA degradation (12). Secondary structure probing revealed that the complementary regions of both RNAs are located in stem-loops SL2 to SL4 of SR4 and in SL3, the 3′ half of P1 and the terminator stem-loop SL4 of *bsrG* RNA. Both L2 of SR4 and L3 of *bsrG* RNA contain 5′ YUNR (U-turn) motifs that were often found to be the scaffold for the initial interaction between sense and antisense RNA (40). Neither deletion of SL2 of SR4

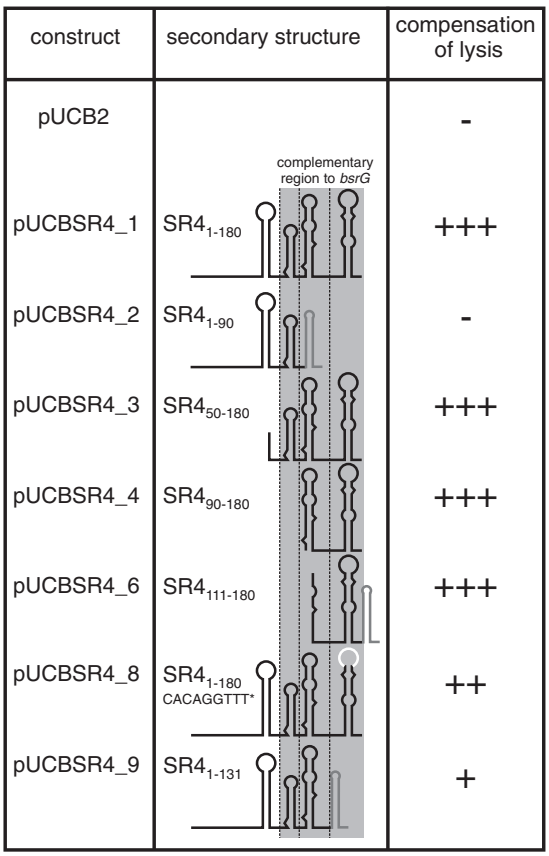

Figure 6. Summary of *in vivo* data. The plasmids listed were used to provide wild-type and mutated SR4 species in trans from plasmid pUCB2 (≈50 copies/cell) to wild-type *bsrG* RNA expressed from plasmid pGKBG (≈15 copies/cell) in a *ΔbsrG*/*Δsr4* background. Test was for lysis at 37°C on agar plates followed by up to 3 days at room temperature (RT). +++, no lysis; ++ lysis after overnight incubation at 37°C followed by 3 days at RT; +, lysis after overnight incubation at 37°C followed by 1 day at RT; −, lysis after overnight incubation at 37°C. The heterologous *bsrF* terminator is drawn in dark grey. Asterisk denotes the sequence by which the wild-type sequence of SR4 was replaced (white line).

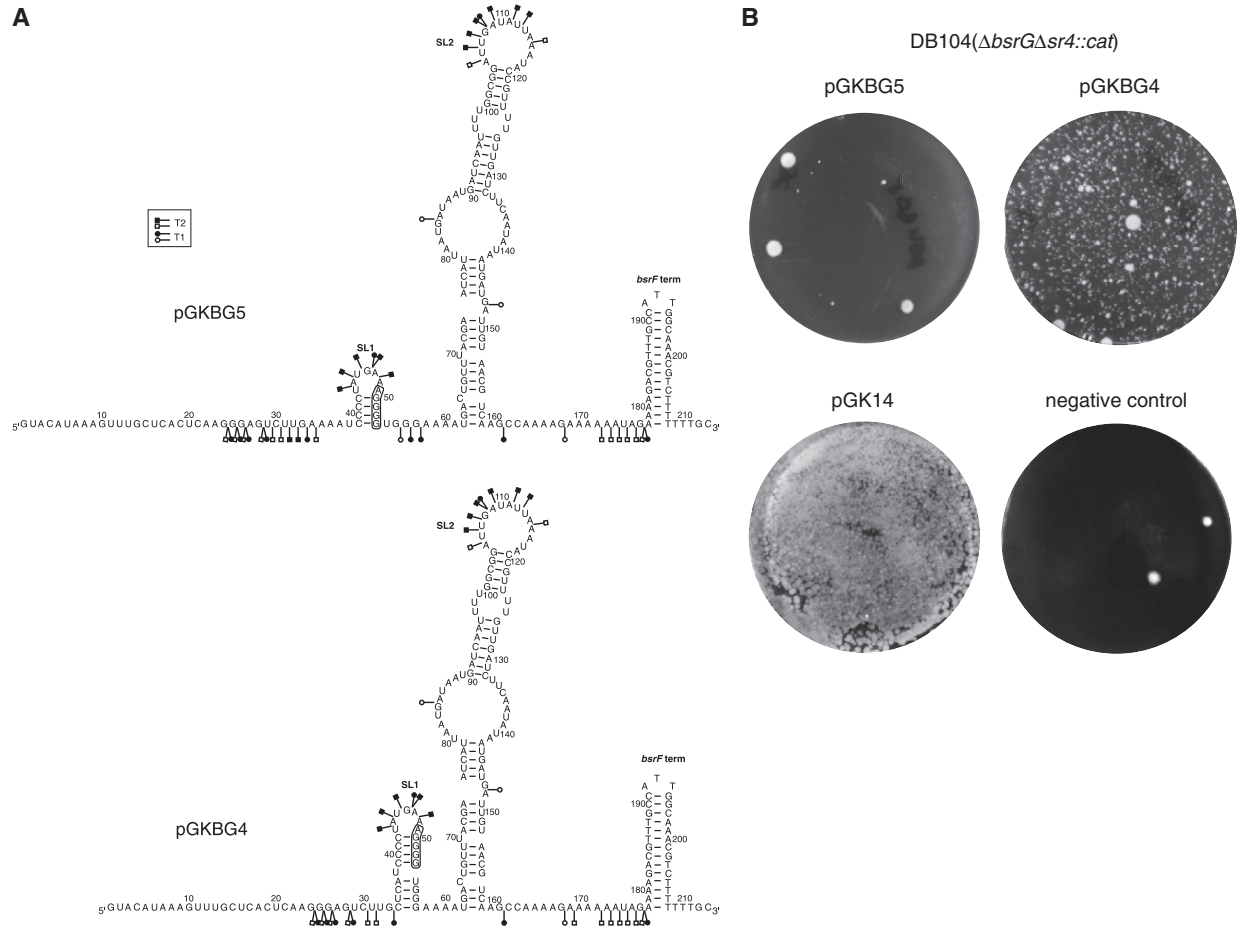

Figure 7. Effect of the *bsrG* expression from plasmids pGKB4 and pGKB5. (**A**) Secondary structures of 3′ truncated *bsrG* RNA species expressed from plasmids pGKBG4 and pGKBG5. Secondary structure probing was performed as in Figure 1 with 5′ labelled *bsrG* RNA and RNases T1 and T2. The corresponding gels are shown in Supplementary Figure S5. Major and minor cuts are denoted by filled and open symbols, respectively. (**B**) Agar plates after transformation with pGKBG4 and pGKBG5. Although pGKBG4 could be established in the *ΔbsrG/Δsr4* strain, but showed lysis after overnight incubation at 37°C, pGKBG5 could not be established. The few non-lysing colonies—comparable with the negative control plate—arouse from spontaneous erythromycin resistance on the chromosome and did not contain plasmids. By contrast, the insert-free vector pGK14 could be established with high frequency and the transformants did not lyse.

(Figure 4) nor of complementary SL4 of *bsrG* RNA (Supplementary Figure S2) had any effect on efficient pairing, indicating that in the case of SR4 L2, a U-turn may not form and recognition between antisense and sense (toxin) RNA occurs elsewhere. By contrast, replacement of L3 of *bsrG* RNA led to a 10-fold decrease of the pairing rate constant (Supplementary Figure S2), and L3 was found to be critical for the initial interaction with SR4 (Figure 5). These results suggest that L3 of *bsrG* RNA may form a U-turn similar to the target RNAs of plasmid pIP501 (34) and *hok*/Sok of plasmid R1 (40), for which U-turns were confirmed experimentally.

Complex formation studies with labelled SR4 and unlabelled *bsrG* RNA and *vice versa* yielded a pairing rate constant of $\approx 6 \times 10^5\,M^{-1}s^{-1}$, which is within the order of magnitude calculated for other *cis*-encoded antisense RNAs (37). Efficient duplex formation required the entire terminator stem-loop SL4 of SR4 and part of SL3. *In vivo* experiments substantiated the *in vitro* results (Figure 6). Full-length SR4 with an altered L4 sequence was impaired in lysis compensation, although to a somewhat lesser extent than an SR4 mutant lacking SL4, whereas a mutant with wild-type L4 comprising only nt 111–180 could perfectly complement lysis.

The initial contact between antisense and sense RNA can either occur between two complementary loops (as in many plasmid replication control systems) or between a loop and a single-stranded region [e.g. *hok*/Sok or RNA-IN/RNA-OUT of IS10, reviewed in (37)]. Owing to accumulating torsional stress, simple helix progression in both directions is topologically impossible in loop–loop contacts. Therefore, such systems require a subsequent interaction at a distal site to circumvent this limitation as shown for CopA/CopT of plasmid R1 [e.g. (41)]. This is clearly supported by a 13-fold higher k_{app} value for $SR4_{111–183}$ compared with $SR4_{128–180}$ (Figure 4A). A combination of RNA–RNA interaction assays (Figure 4) and a time-course experiment (Figure 5) demonstrated that the initial contact occurs between L4 of SR4 and L3 of *bsrG* RNA and intermolecular helix formation progresses via the single-stranded region between SL4 and SL3 towards L3 of SR4 that, afterwards, interacts with the 3′ arm of the

bsrG RNA helix P1 at nt 242–247. Finally, L2 of SR4 pairs with the *bsrG* terminator SL4, but this interaction is not required for stable complex formation. The exchange of either the SR4 L4 sequence or the *bsrG* L3 sequence reduced binding drastically, whereas compensatory mutations restored efficient binding (Figure 4A and Supplementary Figure S2), corroborating the proposed interaction pathway. The exclusive exchange of SR4 L3 did not affect binding to *bsrG* RNA (see Fig. 4A), further substantiating a single loop–loop contact as first contact. So far, it is not known how the double-stranded region in *bsrG* mRNA contacted by L3 of SR4 melts to facilitate this interaction. As shown previously, the RNA chaperone Hfq is not involved, as it was not needed for the inhibitory effect of SR4 (12).

In contrast to *bsrG*/SR4, we found previously for the replication control system of streptococcal plasmid pIP501 (RNAIII/RNAII) that two loop–loop pairs interact simultaneously, and neither of them could be deleted or mutated (20). The same was observed for *E. coli ibs*/Sib (8): Two regions—TRD1 pairing within the toxin ORF and TRD2 complementary to the ribosome binding site (RBS)—both containing single-stranded loops and adjacent double-stranded regions were equally required for initial target recognition. Although for *txpA*/RatA, the secondary structures of both RNAs and that of the complex have been determined, the binding pathway has not been investigated (11). The *txpA*/RatA complex is—as the *bsrG*/SR4 complex (Figure 3)—a complete duplex. By contrast, the final *ibsC*/SibC complex is not a fully paired duplex (8), similar to those found in other systems [reviewed in (37,42)].

As in previous northern blots, even in the presence of the antitoxin SR4, considerable amounts of *bsrG* RNA were detected (12), we asked how the promotion of *bsrG* RNA degradation by SR4 can suffice to prevent toxin synthesis. As we show here, a 4 bp double-stranded region sequesters the RBS in free *bsrG* RNA (Figure 2). The location of ribosome binding sites in double-stranded regions was also found by structure probing for other toxin RNAs, e.g. *B. subtilis txpA* RNA (11), *E. faecalis fst* RNA (43), *E. coli tisB* (4) and *ibsC* RNAs (8) and predicted for the *B. subtilis bsrE* and *bsrH* mRNAs (15). Most likely, this is one important mechanism to reduce toxin translation. *Bacillus subtilis yonT* has instead a weaker GUG start codon, which could fulfil the same purpose. Furthermore, the SD sequences of *txpA* and also of *yonT* mRNA have with 12 and 11 potential bp, respectively, the most extensive complementarities of all *B. subtilis* mRNAs with the anti-SD of the 16S rRNA, which may lead to slow ribosome release rates (15). By contrast, in *E. coli hok*/Sok, the 3′ and 5′ ends of the *hok* mRNA base pair giving rise to a fold-back inhibitory structure (*fbi*), which sequesters the RBS (29), and 3′ exoribonucleolytic processing gradually frees the RBS allowing toxin synthesis in the absence of Sok.

Binding of SR4 to *bsrG* RNA induces a conformational change that extends the double strand obstructing the RBS from 4 to 8 bp (Figure 3). Our hypothesis that this might further reduce translation initiation could be confirmed experimentally with plasmids pGKBG5 and pGKBG4 that mimic the 4 and 8 bp double-stranded structures sequestering the RBS, respectively (Figure 7). Therefore, we can conclude that SR4 does not only promote degradation of *bsrG* RNA by an RNase III dependent mechanism (12) but also inhibits translation by inducing a structural change that further impedes ribosome binding. The induction of a conformational change at the target RBS, which inhibits translation initiation by an sRNA that binds far downstream ($\approx$100 nt), was already observed for *B. subtilis* SR1 regulating translation of *ahrC* RNA (36), which indicates that this might be a more common mechanism. By contrast, the *E. coli* RNA antitoxin IstRI binds far upstream of the RBS at a so-called ribosome standby site and inhibits ribosome binding to this site (4).

SR4 is the first identified dual-acting type I antitoxin and, at the same time, the first *cis*-encoded antisense RNA with two clearly separable functions. In Gram-negative bacteria, RNA antitoxins like Sok or IstRI affect primarily toxin mRNA translation by binding to the RBS, and toxin mRNA degradation is the consequence of the initial RNase III cleavage of the resulting duplex. The well-characterized *E. faecalis* antitoxin RNAII shares properties of *cis*- and *trans*-encoded antisense RNAs, as it uses two complementary regions located apart: the 3′ ends and direct repeats at the 5′ end. However, RNAII inhibits only *fst* mRNA translation and does not cause RNA degradation (39). For *B. subtilis txpA*/RatA, so far, only promotion of toxin RNA degradation has been proposed, and the length of the double-stranded region sequestering the *txpA* SD sequence (5 bp) is not altered on binding of RatA (11), making it unlikely that RatA additionally inhibits translation initiation. So far, no experimental data are available on the putative *B. subtilis* toxins *bsrE* and *bsrH*. It remains to be seen whether the investigation of the large number of recently discovered type I TA systems reveals novel mechanisms of antitoxin action.

SUPPLEMENTARY DATA

Supplementary Data are available at NAR Online.

ACKNOWLEDGEMENTS

The authors are grateful to Roland Hartmann and Gerhart Wagner for helpful and critical suggestions.

FUNDING

Deutsche Forschungsgemeinschaft (DFG) BR1552/7-2 in priority program SPP1258/2 (to S. B.) Funding for open access charge: DFG, BR1552/7-2.

Conflict of interest statement. None declared.

REFERENCES

1. Yamaguchi,Y., Park,J.H. and Inouye,M. (2011) Toxin-antitoxin systems in bacteria and archaea. *Annu. Rev. Genet.*, **45**, 61–79.

2. Gerdes,K., Bech,F.W., Jørgensen,S.T., Løbner-Olesen,A., Rasmussen,P.B., Atlung,T., Boe,L., Karlstrom,O., Molin,S. and von Meyenburg,K. (1986) Mechanism of postsegregational killing by the *hok* gene product of the *parB* system of plasmid R1 and its homology with the *relF* gene product of the *E. coli relB operon*. *EMBO J.*, **5**, 2023–2029.
3. Weaver,K.E., Clewel,C.B. and An,F. (1993) Identification, characterization, and nucleotide sequence of a region of *Enterococcus faecalis* pheromone-responsive plasmid pAD1 capable of autonomous replication. *J. Bacteriol.*, **175**, 1900–1909.
4. Darfeuille,F., Unoson,C., Vogel,J. and Wagner,E.G.H. (2007) An antisense RNA inhibits translation by competing with standby ribosomes. *Mol. Cell*, **26**, 381–392.
5. Unoson,C. and Wagner,E.G. (2008) A small SOS-induced toxin is targeted against the inner membrane in *Escherichia coli*. *Mol. Microbiol.*, **70**, 258–270.
6. Kawano,M., Aravind,L. and Storz,G. (2007) An antisense RNA controls synthesis of an SOS-induced toxin evolved from an antitoxin. *Mol. Microbiol.*, **64**, 738–754.
7. Fozo,E.M., Kawano,M., Fontaine,F., Kaya,Y., Mendieta,K.S., Jones,K.L., Ocampo,A., Rudd,K.E. and Storz,G. (2008) Repression of small toxic protein synthesis by the Sib and OhsC small RNAs. *Mol. Microbiol.*, **70**, 1076–1093.
8. Han,K., Kim,K.S., Bak,G., Park,H. and Lee,Y. (2010) Recognition and discrimination of target mRNAs by Sib RNAs, a cis-encoded sRNA family. *Nucleic Acids Res.*, **38**, 5851–5866.
9. Fozo,E.M. (2012) New type I toxin-antitoxin families from "wild" and laboratory strains of *E. coli*. Ibs-Sib, ShoB-OhsC and Zor-Orz. *RNA Biol.*, **9**, 1504–1512.
10. Silvaggi,J.M., Perkins,J.B. and Losick,R. (2005) Small untranslated RNA antitoxin in *Bacillus subtilis*. *J. Bacteriol.*, **187**, 6641–6650.
11. Durand,S., Gilet,L. and Condon,C. (2012) The essential function of *B. subtilis* RNase III is to silence foreign toxic genes. *PLoS Genet.*, **8**, e1003181.
12. Jahn,N., Preis,P., Wiedemann,C. and Brantl,S. (2012) BsrG/SR4 from *Bacillus subtilis* – the first temperature-dependent type I toxin-antitoxin system. *Mol. Microbiol.*, **83**, 579–598.
13. Fozo,E.M., Makarova,K.S., Shabalina,S.A., Yutin,N., Koonin,E.V. and Storz,G. (2010) Abundance of type I toxin-antitoxin systems in bacteria: searches for new candidates and discovery of novel families. *Nucleic Acids Res.*, **38**, 3743–3759.
14. Dörr,T., Vulic,M. and Lewis,K. (2010) Ciprofloxacin causes persister formation by inducing the TisB toxin in *Escherichia coli*. *PLoS Biol.*, **8**, e1000317.
15. Durand,S., Jahn,N., Condon,C. and Brantl,S. (2012) Type I toxin-antitoxin systems in *Bacillus subtilis*. *RNA Biol.*, **9**, 1491–1497.
16. Brantl,S. (2012) Bacterial type I toxin-antitoxin systems. *RNA Biol.*, **9**, 1488–1490.
17. Brantl,S. (2012) Acting antisense: plasmid- and chromosome-encoded sRNAs from Gram-positive bacteria. *Future Microbiol.*, **7**, 853–871.
18. Kwong,S.M., Skurray,R.A. and Firth,N. (2006) Replication control of *staphylococcal* multiresistance plasmid pSK41: an antisense RNA mediates dual-level regulation of Rep expression. *J. Bacteriol.*, **188**, 4404–4412.
19. Brantl,S. and Wagner,E.G.H. (1994) Antisense RNA-mediated transcriptional attenuation occurs faster than stable antisense/target RNA pairing: an *in vitro* study of plasmid pIP501. *EMBO J.*, **13**, 3599–3607.
20. Heidrich,N. and Brantl,S. (2007) Antisense RNA-mediated transcriptional attenuation in plasmid pIP501: the simultaneous interaction between two complementary loop pairs is required for efficient inhibition by the antisense RNA. *Microbiology*, **153**, 420–427.
21. Brantl,S. and Wagner,E.G.H. (2000) Antisense-RNA mediated transcriptional attenuation: an *in vitro* study of plasmid pT181. *Mol. Microbiol.*, **35**, 1469–1482.
22. Asano,K. and Mizobuchi,K. (1998) Copy number control of IncIα plasmid ColIb-P9 by competition between pseudoknot formation and antisense RNA binding at a specific RNA site. *EMBO J.*, **17**, 5201–5213.
23. André,G., Even,S., Putzer,H., Burguière,P., Croux,C., Danchin,A., Martin-Verstraete,I. and Soutourina,O. (2008) S-box and T-box riboswitches and antisense RNA control a sulphur metabolic operon of *Clostridium acetobutylicum*. *Nucleic Acids Res.*, **36**, 5955–5969.
24. Opdyke,J.A., Fozo,E.M. and Storz,G. (2011) RNase III participates in GadY-dependent cleavage of the *gadX-gadW* mRNA.J. *Mol. Biol.*, **406**, 29–43.
25. Kawano,M. (2012) Divergently overlapping cis-encoded antisense RNA regulating toxin-antitoxin systems from *E. coli*: hok/sok, ldr/rdl, symE/symR. *RNA Biol.*, **9**, 1520–1527.
26. Weaver,K.E. (2012) The par toxin-antitoxin system from *Enterococcus faecalis* plasmid pAD1 and its chromosomal homologs. *RNA Biol.*, **9**, 1498–1503.
27. Gerdes,K., Gultyaev,A.P., Franch,T., Pedersen,K. and Mikkelsen,N.D. (1997) Antisense RNA-regulated programmed cell death. *Annu. Rev. Genet.*, **31**, 1–31.
28. Thisted,T., Sørensen,N.S., Wagner,E.G.H. and Gerdes,K. (1994) Mechanism of post-segregational killing: Sok antisense RNA interacts with Hok mRNA via its 5′-end single-stranded leader and competes with the 3′-end of Hok mRNA for binding to the mok translational initiation region. *EMBO J.*, **13**, 1960–1968.
29. Thisted,T., Sørensen,N.S. and Gerdes,K. (1995) Mechanism of post-segregational killing: secondary structure analysis of the entire Hok mRNA from plasmid R1 suggests a fold-back structure that prevents translation and antisense RNA binding. *J. Mol. Biol.*, **247**, 859–873.
30. Greenfield,T.J. and Weaver,K.E. (2000) Antisense RNA regulation of the pAD1 *par* post-segregational killing system requires interaction at the 5′ and 3′ ends of the RNAs. *Mol. Microbiol.*, **37**, 661–670.
31. Greenfield,T.J., Ehli,E., Kirshenmann,T., Franch,T., Gerdes,K. and Weaver,K.E. (2000) The antisense RNA of the *par* locus of pAD1 regulates the expression of a 33-amino-acid toxic peptide by an unusual mechanism. *Mol. Microbiol.*, **37**, 652–660.
32. Kawamura,F. and Doi,R.H. (1984) Construction of a *Bacillus subtilis* double mutant deficient in extracellular alkaline and neutral proteases. *J. Bacteriol.*, **160**, 442–444.
33. Heidrich,N., Chinali,A., Gerth,U. and Brantl,S. (2006) The small untranslated RNA SR1 from the *B. subtilis* genome is involved in the regulation of arginine catabolism. *Mol. Microbiol.*, **62**, 520–536.
34. Heidrich,N. and Brantl,S. (2003) Antisense-RNA mediated transcriptional attenuation: importance of a U-turn loop structure in the target RNA of plasmid pIP501 for efficient inhibition by the antisense RNA. *J. Mol. Biol.*, **333**, 917–929.
35. Licht,A., Preis,S. and Brantl,S. (2005) Implication of CcpN in the regulation of a novel untranslated RNA (SR1) in *B. subtilis*. *Mol. Microbiol.*, **58**, 189–206.
36. Heidrich,N., Moll,I. and Brantl,S. (2007) *In vitro* analysis of the interaction between the small RNA SR1 and its primary target *ahrC* mRNA. *Nucleic Acids Res.*, **35**, 4331–4346.
37. Brantl,S. (2007) Regulatory mechanisms employed by cis-encoded antisense RNAs. *Curr. Opin. Microbiol.*, **10**, 102–109.
38. Gerdes,K. and Wagner,E.G.H. (2007) RNA antitoxins. *Curr. Opin. Microbiol.*, **10**, 117–124.
39. Weaver,K.E., Ehli,E.A., Nelson,J.S. and Patel,S. (2004) Antisense RNA regulation by stable complex formation in the *Enterococcus faecalis* plasmid pAD1 *par* addiction system. *J. Bacteriol.*, **186**, 6400–6408.
40. Franch,T., Petersen,M., Wagner,E.G.H., Jacobsen,J.P. and Gerdes,K. (1999) Antisense RNA regulation in prokaryotes: rapid RNA/RNA interaction facilitated by a general U-turn loop structure. *J. Mol. Biol.*, **294**, 1115–1125.
41. Kolb,F.A., Engdahl,H.M., Slagter-Jäger,J.G., Ehresmann,B., Ehresmann,C., Westhof,E., Wagner,E.G. and Romby,P. (2000) Progression of a loop-loop complex to a four-way junction is crucial for the activity of a regulatory antisense RNA. *EMBO J.*, **19**, 5905–5915.
42. Wagner,E.G.H. and Brantl,S. (1998) Kissing and stability in the control of plasmid replication. *Trends Biochem. Sci.*, **23**, 451–454.
43. Shokeen,S., Patel,S., Greenfield,T.J., Brinkman,C. and Weaver,K.E. (2008) Translational regulation by an intramolecular stem-loop is required for intermolecular RNA regulation of the *par* addiction module. *J. Bacteriol.*, **190**, 6076–6083.